



Society of Petroleum Engineers

SPE-205267-MS

Characterize Fracture Development Through Strain Rate Measurements by Distributed Acoustic Sensor DAS

Jin Tang and Ding Zhu, Texas A&M University

Copyright 2022, Society of Petroleum Engineers DOI [10.2118/205267-MS](https://doi.org/10.2118/205267-MS)

This paper was prepared for presentation at the SPE International Hydraulic Fracturing Technology Conference & Exhibition, Muscat, Oman, 11 - 13 January 2022.

This paper was selected for presentation by an SPE program committee following review of information contained in an abstract submitted by the author(s). Contents of the paper have not been reviewed by the Society of Petroleum Engineers and are subject to correction by the author(s). The material does not necessarily reflect any position of the Society of Petroleum Engineers, its officers, or members. Electronic reproduction, distribution, or storage of any part of this paper without the written consent of the Society of Petroleum Engineers is prohibited. Permission to reproduce in print is restricted to an abstract of not more than 300 words; illustrations may not be copied. The abstract must contain conspicuous acknowledgment of SPE copyright.

Abstract

In multistage hydraulic fracturing treatments, the combination of extreme large-scale pumping (high rate and volume) and the high heterogeneity of the formation (because of large contact area) normally results in complex fracture growth that cannot be simply modeled with conventional fracture models. Lack of understanding of the fracturing mechanism makes it difficult to design and optimize hydraulic fracturing treatments. Many monitoring, testing and diagnosis technologies have been applied in the field to describe hydraulic fracture development. Strain rate measured by distributed acoustic sensor (DAS) is one of the tools for fracture monitoring in complex completion scenarios. DAS measures far-field strain rate that can be of assistance for fracture characterization, cross-well fracture interference identification, and well stimulation efficiency evaluation. Many field applications have shown DAS responses on observation wells or surrounding producers when a well in the vicinity is fractured. Modeling and interpreting DAS strain rate responses can help quantitatively map fracture propagation.

In this work, a methodology is developed to generate the simulated strain-rate responds to assumed fracture systems. The physical domain contains a treated well that the generate strain variation in the domain because of fracturing, and an observation well that has fiber-optic sensor installed along it to measure the strain rate responses to the fracture propagation. Instead of using a complex fracture model to forward simulate fracture propagation, this work starts from a simple 2D fracture propagation model to provide hypothetical fracture geometries in a relatively reasonable and acceptable range for both single fracture case and multiple fracture case. Displacement discontinuity method (DDM) is formulated to simulate rock deformation and strain rate responds on fiber-optic sensors. At each time step, fracture propagation is first allowed, then stress, displacement and strain field are estimated as the fracture approaches to the observation well. Afterward, the strain rate is calculated as fracture growth to generate patterns as fracture approaching. Extended simulation is conducted to monitor fracture propagation and strain rate responses. The patterns of strain rate responses can be used to recognize fracture development.

Examples of strain rate responses for different fracturing conditions are presented in this paper. The relationship of injection rate distribution and strain rate responses is investigated to show the potential of using DAS measurements to diagnose multistage hydraulic fracturing treatments.

Introduction

Hydraulic fracture monitoring techniques have been applied to diagnose fracture propagation, especially in unconventional reservoir development, where multistage, massive fracture treatments are applied. Distributed acoustic sensing (DAS) is one of the fracture monitoring techniques that enables continuous detection of acoustic and vibration variations during fracturing along the entire wellbore in real-time. The application of distributed acoustic sensing can be divided into two groups: high frequency and low frequency. DAS data in high-frequency band (200Hz-7000Hz) have been applied in wellbore and near-wellbore stimulation and production monitoring. The applications include liquid holdup estimation for two-phase flow in pipe (Bukhamsin and Horne, 2014), fracture fluid distribution interpretation during fracturing (Pakhotina et al., 2020a), near-wellbore evaluation of perforation cluster efficiency (Ugueto C. et al., 2016), evaluation of perforation erosion (Pakhotina et al., 2020b), as some examples.

Low-frequency DAS monitoring (<1 Hz) have been studied for the events related to geo-mechanical event detection that provides information for fracture characterization (Jin and Roy, 2017; Ugueto et al., 2019; Li et al., 2020). This application usually uses fiber optic sensors that are installed on an observation well in the vicinity of a well that is going to be fractured. During fracture pumping, strain field variation caused by fracture propagation can be observed by the sensor on the offset well. Raw DAS data is recorded at a high sampling rate. The raw DAS data is down-sampled at a lower frequency and stored as raw low-frequency DAS data. The processed low-frequency DAS data contain the information regarding geo-mechanical events in strain-rate polarity that can help to better understand fracture development.

In this paper, we develop an integrated approach to simulate far-field strain rate responses along a monitoring well during fracture treatment on an injection well, and investigate the DAS response characteristics as fractures develop. We use this information to describe fracture propagation.

Methodology

An integrated methodology is developed to simulate the far-field strain rate behavior on fiber optic sensor during hydraulic fracturing. The general workflow of this simulation study is to estimate fracture geometries using the KGD model with fluid leakoff considered (Valko and Economides, 1995), and then use displacement discontinuity method to simulate the stress and displacement in the stimulation domain based on the hypothetical fracture growth. The model will transform the stress and displacement into strain based on rock deformation theory. For field application, we use averaged value over sensor gauge length to generate strain from fiber-optic sensor measurements. Strain rate is simulated in time domain by taking the difference of strain value at each time step. The simulated strain rate is then transformed into polarized patterns by applying a special data processing. These patterns can be used in interpreting low-frequency DAS measurements to understand fracture development in multi-cluster fracturing.

The physical domain shown in Figure 1 is used in the study. The domain contains two wells, one for injection, and one for monitoring. Fiber-optic sensor is considered to be permanently deployed outside the casing of the monitoring well.

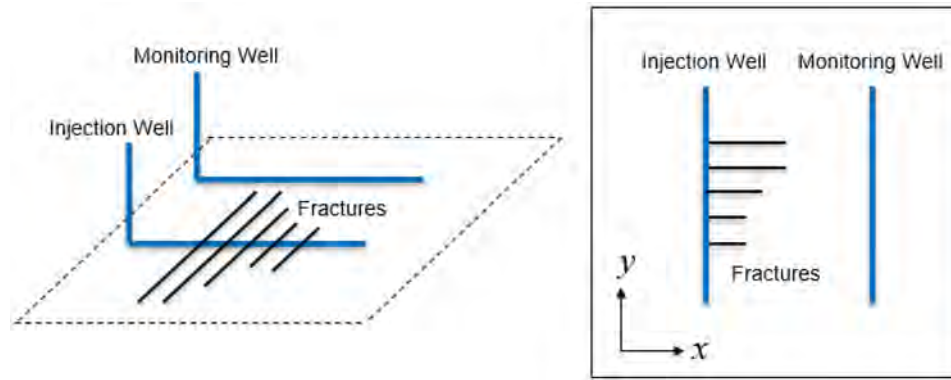


Figure 1—Schematic of the defined problem

Displacement Discontinuity Method

Crouch (1976) developed the displacement discontinuity method, a special boundary element method also commonly referred as DDM, to calculate the stress and displacement around a fracture with arbitrary shape in a linear elastic domain. This method has been used to solve geo-mechanical problem (Crouch, 1983; Wu, 2014). The objective is to simulate the far-field strain rate along the monitoring well while the injection well is fractured (Figure 1). The propagating fracture is assumed to be perfectly aligned with x -axis and perpendicular to the injection well, and therefore, only normal stresses in both the x and y direction (σ_{xx} , σ_{yy}) and the displacements in the y direction (u_y) are needed for the strain simulation. Shear stresses (σ_{xy}) and displacements in the x direction (u_x) are neglected in this study. With these assumptions, the problem can be simplified for single-fracture case as shown in Figure 2, a vertical fracture locates in the center of the domain, and the fracture is discretized into multiple elements.

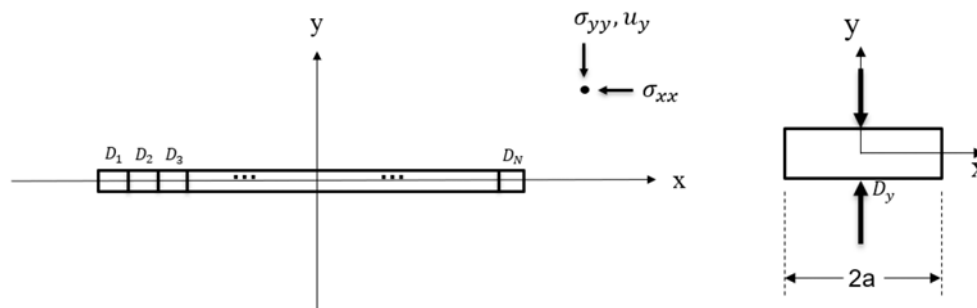


Figure 2—Illustration of a discretized two-dimensional vertical fracture (left) and its element (right)

Because of the fracture is vertical in the y -direction, there are only displacement discontinuities in the y direction (D_y) and no displacement discontinuities in the x direction (D_x) along the fracture. Therefore, Crouch's method for the defined problem is a solution of displacement discontinuity method becomes a solution for a point source. For n^{th} element, its induced stresses, σ , and displacement, u , at a position (x, y) is given as,

$$\sigma_{xx}^n = 2GD_y^n [f_{,yy} + \bar{y}_n f_{,yyy}] \quad (1)$$

$$\sigma_{yy}^n = 2GD_y^n [f_{,yy} - \bar{y}_n f_{,yyy}] \quad (2)$$

$$u_y^n = D_y^n [2(1-\nu) f_{,y} - \bar{y}_n f_{,yyy}] \quad (3)$$

where D_x and D_y are displacement discontinuities in the x and y direction respectively, and G is shear modulus,

$$G = \frac{E}{2(1+\nu)} \quad (4)$$

where E is Young's modulus, and ν is Poisson's ratio.

Each element will be calculated in its location coordinate system. The local coordinate of the n^{th} element is,

$$\bar{x}_n = x - x_n, \quad n = 1, 2, 3, \dots, N \quad (5)$$

$$\bar{y}_n = y - y_n, \quad n = 1, 2, 3, \dots, N \quad (6)$$

where N denotes the number of elements in the fracture.

Only the following derivatives of the function $f(x, y)$ are needed for the calculation of the simplified problem,

$$f_{,y} = \frac{-1}{4\pi(1-\nu)} \left[\arctan \frac{\bar{x}_n + a}{\bar{y}_n} - \arctan \frac{\bar{x}_n - a}{\bar{y}_n} \right] \quad (7)$$

$$f_{,yy} = \frac{-1}{4\pi(1-\nu)} \left[\frac{\bar{x}_n - a}{(\bar{x}_n - a)^2 + \bar{y}_n^2} - \frac{\bar{x}_n + a}{(\bar{x}_n + a)^2 + \bar{y}_n^2} \right] \quad (8)$$

$$f_{,yyy} = \frac{2\bar{y}_n}{4\pi(1-\nu)} \left[\frac{\bar{x}_n - a}{\{(\bar{x}_n - a)^2 + \bar{y}_n^2\}^2} - \frac{\bar{x}_n + a}{\{(\bar{x}_n + a)^2 + \bar{y}_n^2\}^2} \right] \quad (9)$$

Thus, the induced stress by the fracture at any point (x, y) in the domain can be expressed as,

$$\sigma_{xx} = \sum_{n=1}^N G^n \sigma_{xx}^n \quad (10)$$

$$\sigma_{yy} = \sum_{n=1}^N G^n \sigma_{yy}^n \quad (11)$$

$$u_y = \sum_{n=1}^N G^n u_y^n \quad (12)$$

The 2D DDM assumes that only plane strain exists and fracture height is infinite. To enhance the reality of the fracture, we adopt a 3D correction factor G^n derived by Olson (2004) that transform an infinite fracture height to a finite fracture height in 2D DDM calculation,

$$G^n = 1 - \frac{d_n^\beta}{\left[d_n^2 + \left(\frac{h}{\alpha} \right)^2 \right]^{\frac{\beta}{2}}} \quad (13)$$

where $\alpha = 1$ and $\beta = 2.3$ are empirical constants, h is the fracture height, and d_n is defined as,

$$d_n = \sqrt{\bar{x}_n^2 + \bar{y}_n^2} \quad (14)$$

Strain Rate Calculation for Multiple Fractures

The objective of this study is to investigate the far-field strain rate behavior at fiber-optic sensors locations in a nearby well during hydraulic fracturing, and detect the fractures propagate from injection well to monitoring well from strain rate behavior.

To obtain the far-field strain rate data on fiber-optic sensors, an imaginary offset well is set in the simulated domain parallel to the injection well with a giving well spacing, as shown in Figure 3.

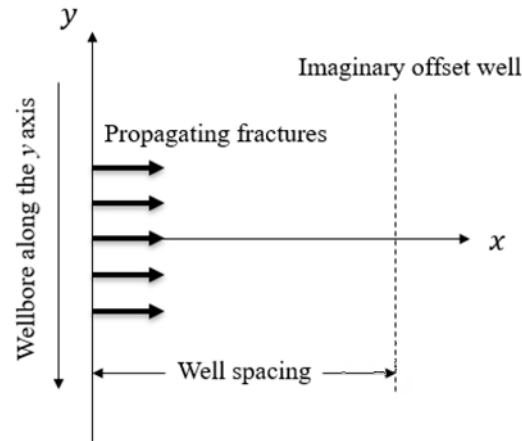


Figure 3—Schematic of cross-well monitoring for the fracture treatment

To start the solution of the problem, we use the KGD model with fluid leakoff considered to create fractures under certain injection conditions. Each fracture is propagated separately, and the only connection between the fractures is through leakoff. Once the fracture is created, fracture width serves as discontinuity, stress, displacement and strain profiles can be generated from the equations presented before. Recording the stress and displacement value at the imaginary offset well at all time steps, strain based on rock-deformation. The rock-deformation based strain tracks strain changes over the coordinate system of computation (in x - y space). For field application, we calculate strain based on fiber-optic sensor measurement with an average strain over the sensor gauge length.

Strain Rate Simulation Based on Rock Deformation.

In two-dimensional elasticity, plane stress is the stress is the only stress that is restricted to a single plane. Thus, the axial plain strain, ε_{yy} , can be determined as,

$$\varepsilon_{yy} = \frac{(1-\nu^2)}{E} \left[\sigma_{yy} - \frac{\nu}{1-\nu} \sigma_{xx} \right] \quad (15)$$

where σ_{xx} and σ_{yy} are plane stresses in different directions from Equations 10 and 11, E is Young's modulus, and ν is Poisson's ratio.

Strain Rate Simulation Based on Fiber-Optic Measurement.

For permanently installed fiber-optic sensors, we assume that with good cementing, the fiber-optic sensors are mechanically coupled with the formation. The strain rate variations of formation due to hydraulic fracturing can be measured by the optical fiber. However, the strain measurements by fiber-optic sensors are the difference of displacement over a gauge length. DAS generates digital waveforms at each channel that are not a point measurement but are strain changes measured over a spatial distance. This distance is referred to as gauge length (Dou et al., 2017). Gauge length should not be confused with spatial resolution, which is a measurement performance parameter. The gauge length of DAS varies depending on the vendors. Fiber optic sensor measured strain over a gauge length can be expressed as,

$$\varepsilon_{yy} = \frac{u_y^{(j+\frac{1}{2}GL)} - u_y^{(j-\frac{1}{2}GL)}}{GL} \quad (16)$$

where u_y is the positional displacement vector in direction y parallel to the offset well, with the superscripts indicating positions, j indicates positions along the fiber, and GL is the fiber's gauge length. u_y is calculated by Equation 12.

Strain Rate Calculation.

Strain rate can be simulated in the time domain by taking the difference of strain value at the imaginary offset well at each time step and then applying the following equation,

$$\dot{\varepsilon} = \frac{\varepsilon^{n+1} - \varepsilon^n}{t^{n+1} - t^n} \quad (17)$$

where $\dot{\varepsilon}$ is strain rate, ε is strain, t is time, and n represents the time index.

In summary, to establish the relationship between a propagating fracture and DAS responses on a nearby monitoring well, we start with a fracture geometry that is calculated with 2D analytical model (KGD model), and then use 2D displacement discontinuity method to relate fracture geometry to the stress/strain change due to the fracture propagation. Finally strain rates based on rock deformation theory, also for sensor measurements, are calculated over the time space.

Model Application Examples

We start with a single-fracture case to illustrate the calculation of strain rates. Figure 4 shows the physical domain of a single fracture propagating to the offset well during fracture pumping. The simulation domain is 400 ft by 1500 ft. The distance between the fractured well and imaginary well is 600 ft. The rest of the input used in simulation is listed in Table 1.

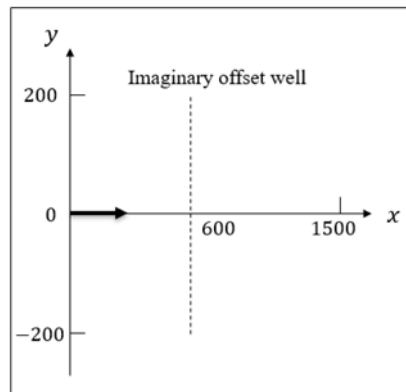


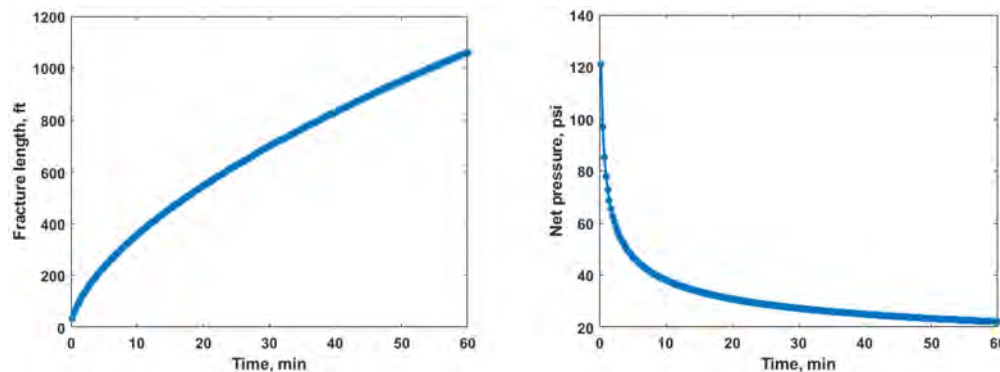
Figure 4—The stimulation domain for the single fracture case study

Table 1—Input data for strain rate simulation of the single fracture case study

Parameter	Value
Young's modulus, psi	4350000
Poisson's ratio, [-]	0.2
Injection rate per one wing, bbl/min	20
Fluid viscosity, cp	5
Fracture height, ft	200
Injection time, min	60
Leak-off coefficient, ft/min ^{0.5}	0.001
Domain dimension, ft	400×1500
Well spacing, ft	600
Gauge length, m	2

In this paper, we assume that the bi-wing hydraulic fracture is symmetrical extending to each side of the wellbore. Because we only interested in the strain response on fiber optic sensor that is installed on the offset well, we only demonstrate calculation on one wing of the propagating fracture.

We first simulate fracture width, half-length and net pressure evolution over time. The simulation results of the length and net pressure are shown in Figure 5. The fracture width distribution is then used to calculate the strain rate.

**Figure 5—Fracture half-length (left) and net pressure (right) evolution over time**

Rock Deformation Based Strain.

The stress distribution calculated from the width distribution at the fracture location ($y=0$) at different time step is shown in Figure 6 as a 2D contour plot (waterfall plot). The vertical axis is depth, and the horizontal axis is time. The color intensity indicate the level of the parameter on the plot. Figure 6(a) shows when the fracture starts to propagate from the treated well, but still far away from the offset well, with fracture length of 200 ft (3.9 minutes of pumping). Figure 6(b) shows that the fracture is approaching the offset well with a fracture length of 500 ft at 17.4 minutes of pumping time. Figure 6(c) is the strain response at the moment when fracture actually arrives at the offset well at 23.4 minutes. Figure 6(d) shows when the fracture has intercepted the offset and passes through it. The fracture length is 1000 ft at 55.4 minutes. Figure 7 displays the stresses along the imaginary well as a function of time.

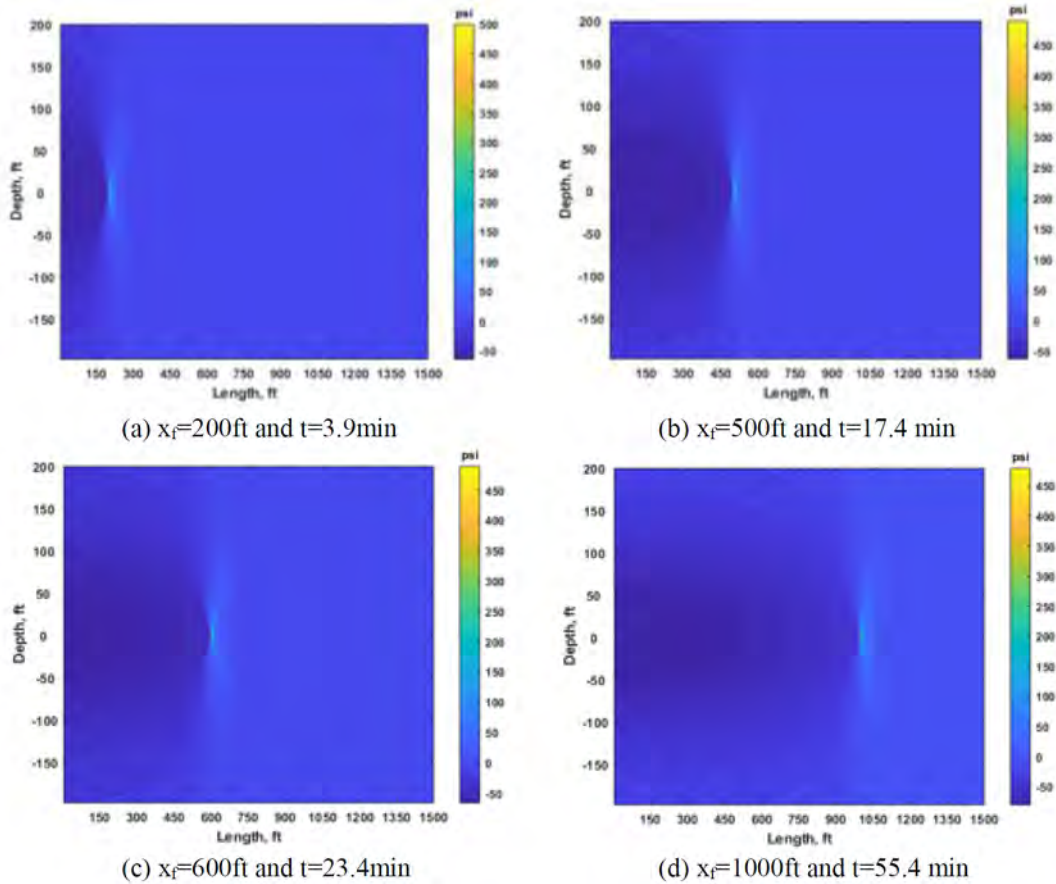


Figure 6—Stress domain at different time step with different fracture half-length

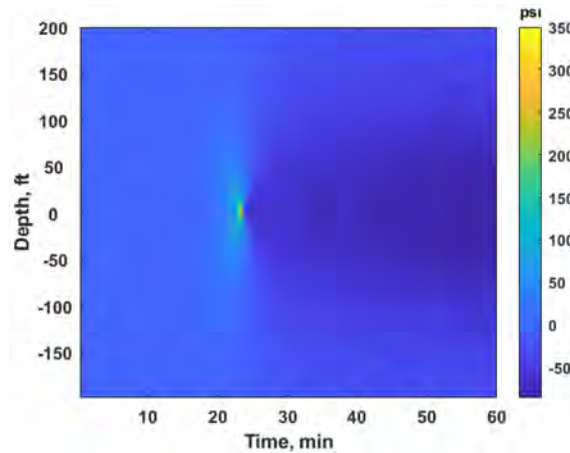


Figure 7—Stress evolution at fiber location over time

Once obtaining the stress information, we convert the stress to strain by using Equation 15. Same as the stress results, the strain results are displayed at the fracture location at different time steps with fracture lengths as a parameter, as shown in Figure 8. Figure 9 is the strain response to fracture propagation along the imaginary well (monitoring well) as a function of time based on rock deformation theory. The strain rate profile is calculated from the strain history, and displayed in Figure 10. This is the strain rate based on the rock deformation theory.

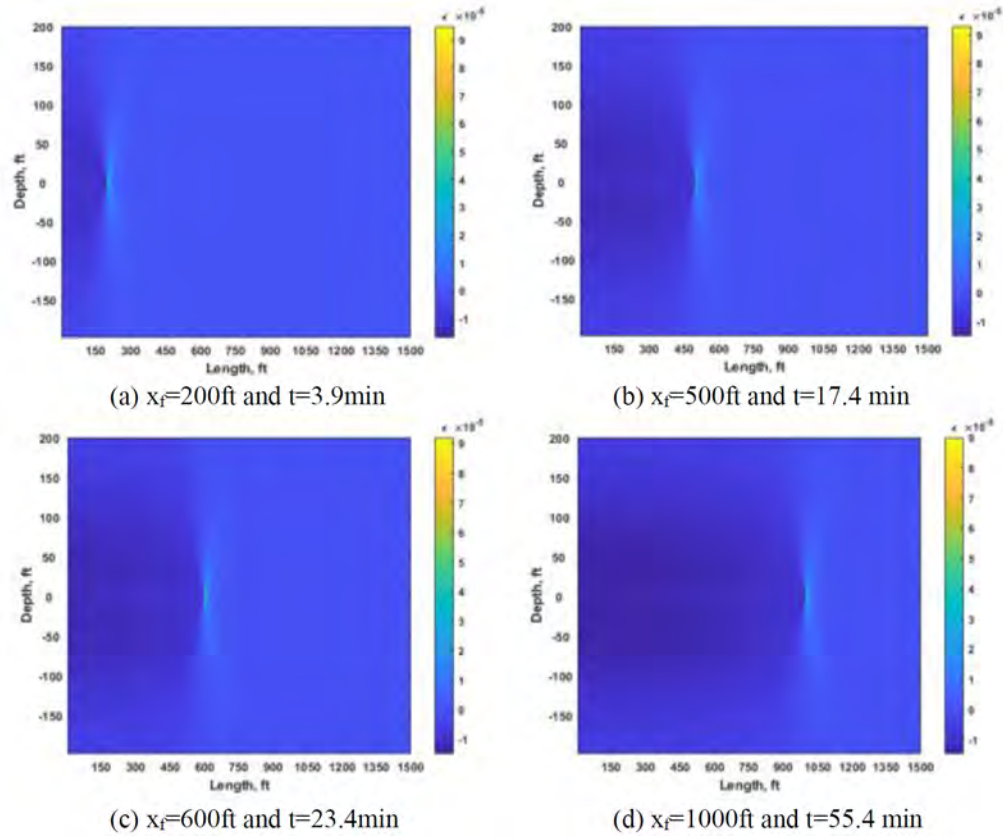


Figure 8—Strain domain based on rock deformation at different time step with different fracture half-length

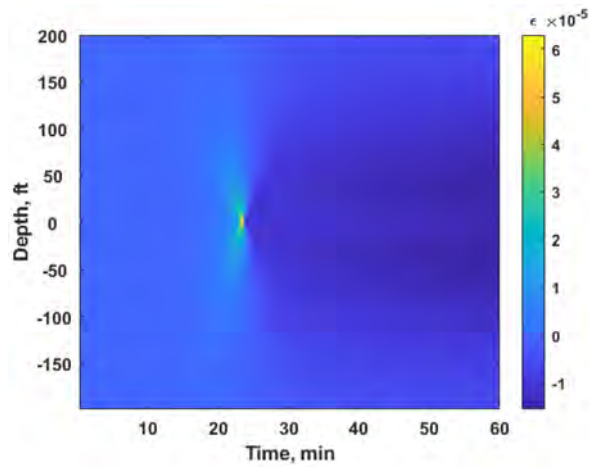


Figure 9—Strain based on rock deformation evolution at fiber location over time

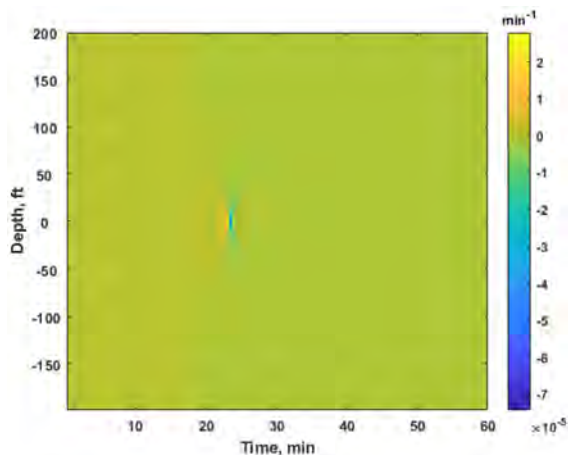


Figure 10—Strain rate based on rock deformation evolution at fiber location over time

Strain Rate on Fiber Optic Sensor Measurements.

Strain rate based on fiber-optic sensor measurements is calculated from displacements (Equation 12). The gauge length used in the example is 10 meters. We calculate the displacement distribution change as a function of time first, and the results are shown in Figure 11. Same time step/fracture lengths are used here as the ones used in the rock deformation based cases. The fracture length selected for calculation are 200 ft at 3.9 minutes in Figure 11(a), 500 ft at 17.4 minutes in Figure 11(b), 600 ft (at the moment fracture intercept the monitoring well) at 23.4 minutes in Figure 11(c) and 1000 ft (fracture passes the monitoring well) at 55.4 minutes in Figure 11(d). Figure 12 shows the displacements along the imaginary monitoring well as a function of time.

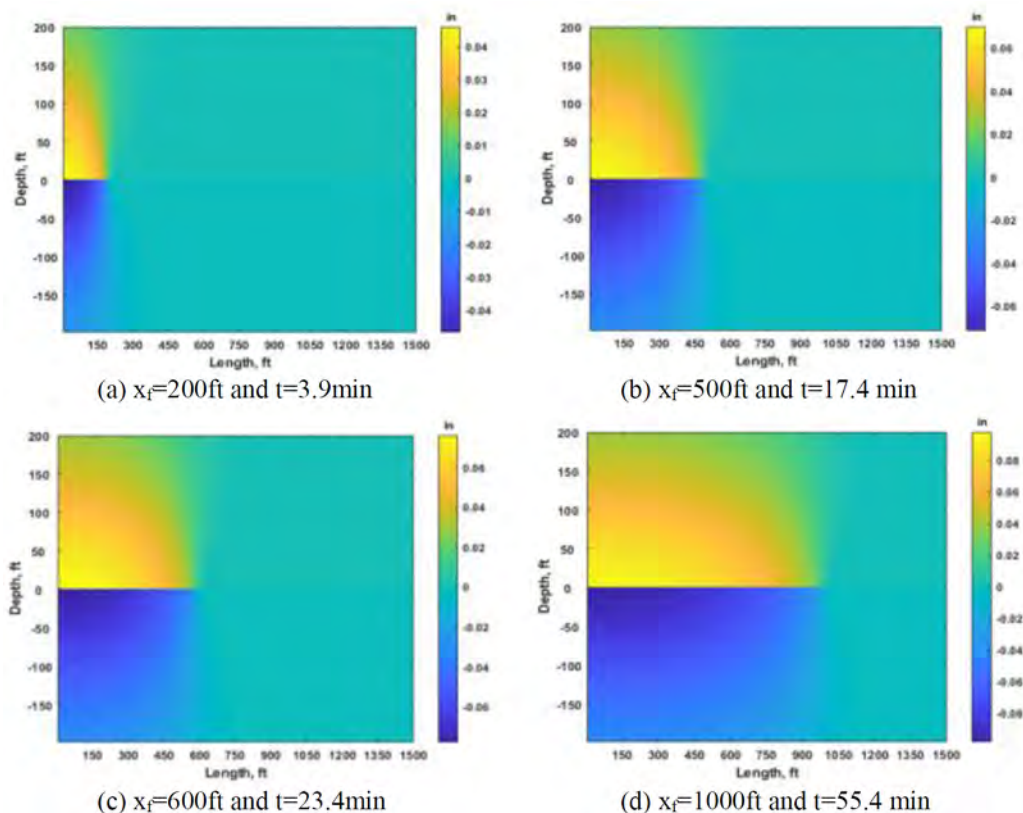


Figure 11—Displacement at different time step with different fracture half-length

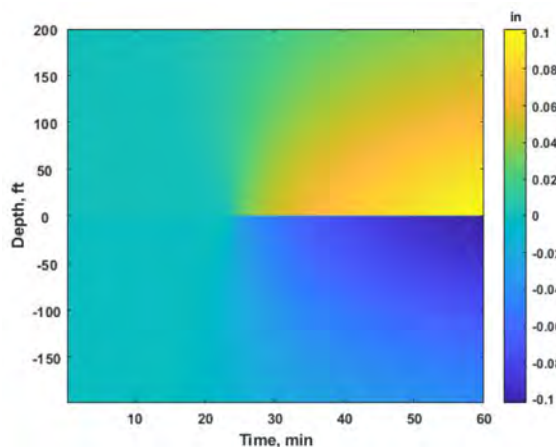


Figure 12—Displacement evolution at fiber location over time

The displacements are then transformed to the strain based on fiber-optic measurement by using Equation 16. The four corresponding strain calculated from the displacements are shown in Figure 13. The lengthening of the "yellow strip" on the pictures in Figure 13 indicates the extension of the fracture.

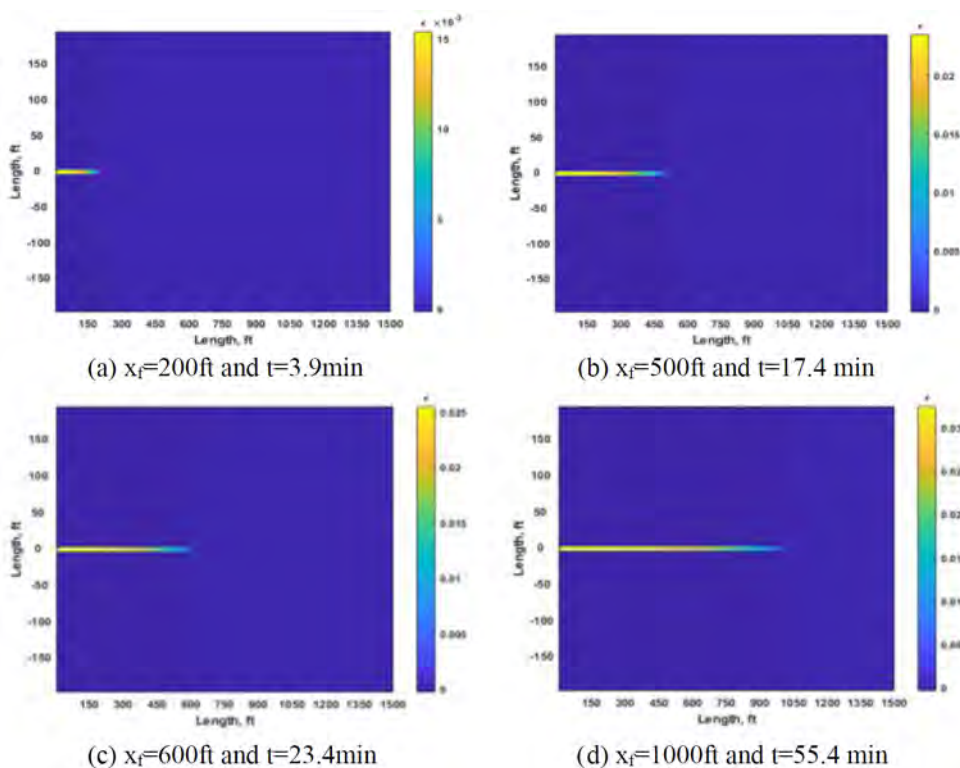


Figure 13—Strain domain based fiber-optic sensor measurement at different time step

The strain along the imaginary monitoring well as a function of time based on fiber-optic measurements is shown in Figure 14. This can be easily convert to strain rate by Equation 17. The strain rate result for this case is shown in Figure 15.

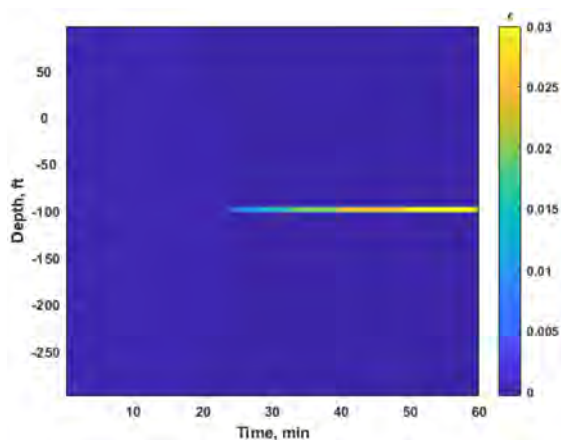


Figure 14—Strain evolution based on fiber-optic measurement at fiber location over time

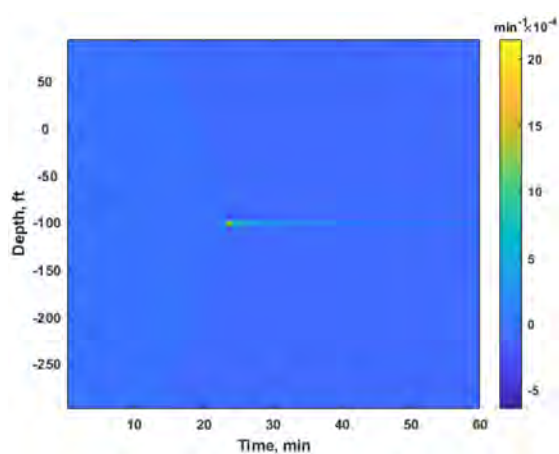


Figure 15—Strain rate based on fiber-optic measurement at fiber location over time

Characterization of Strain Rate Responses to Fracture Propagation

Noticed that in Figure 15, the result of the strain rate as a function of time is not very distinguishable because of the wide range of the raw data. We process the following procedure to the data to enhance information visibility. We first magnify the raw strain rate data with a linear scale by multiplying a large number. In this study, the strain rate $\dot{\epsilon}$ is enlarged by 10^9 . The enlarged strain rate data, marked as $\tilde{\epsilon}$, are transformed into a logarithmic scaled number under the following rules,

$$\hat{\epsilon} = \begin{cases} \log(\tilde{\epsilon}), & \tilde{\epsilon} > 1 \\ 0, & -1 \leq \tilde{\epsilon} \leq 1 \\ -\log(-\tilde{\epsilon}), & \tilde{\epsilon} < -1 \end{cases} \quad (18)$$

For the objective of this study, we will only discuss the result of fiber optic sensor based strain behavior. The detailed discussion for rock deformation based result can be found in Tang (2021). Figure 16 shows a strain rate plot as a function of time. The gauge length used in this example is 10 meters. It is clear that there is not enough feature that can be used for fracture diagnosis. Once the transformation procedure is applied to the strain rate results, Figure 17 shows distinct responses of strain rate to fracture propagation. Before the fracture arrives the monitoring well, the pattern shows a "cone shape". After the fracture intercepts with the monitoring well where the DAS cable is installed, the pattern changes from the tip of the "cone" to a "strip", as the fracture continues to extend.

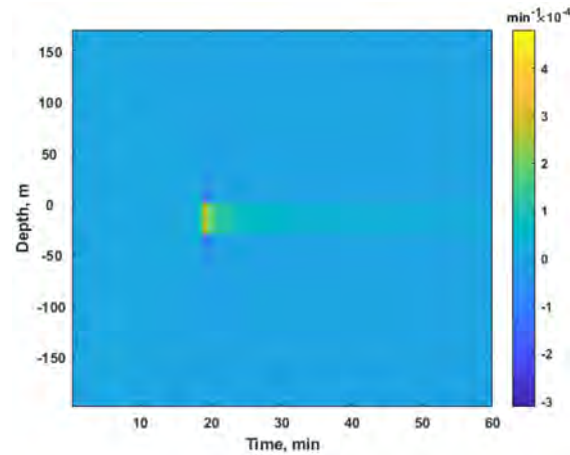


Figure 16—Strain rate based on fiber-optic measurements over time

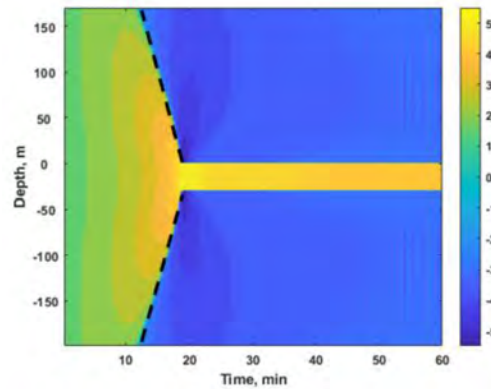


Figure 17—Processed strain rate based on fiber-optic measurements over time

A dashed lines marked in Figure 17 is defined as the slope of the "cone shape" when assuming a linear boundary between the extending zone (yellow colored) and the compressing zone (blue colored). Because the upper part and lower part of the "cone shape" are symmetric in this case, an absolute value is used as the slope of the cone shape. The parametric study shows that the magnitude of the slope is related to the propagation velocity or the injection rate of fracturing. An empirical correlation is developed to describe this relationship. The system used to develop the correlation is shown in Figure 18, and the input data is listed in Table 2. Since fracture propagation rate is directly related to injection rate, the injection rate is used as the parameter for the correlation. Four different injection rates, 10 bbl/min, 15 bbl/min, 20 bbl/min, and 25 bbl/min, are used to generate waterfall plot for strain rate and the slope for each cone shape is estimated to build the correlation.

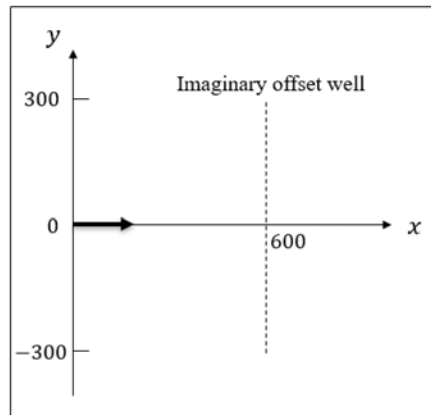


Figure 18—Stimulation domain for the empirical correlation study

Table 2—Input data for the empirical correlation study

Parameter	Value
Young's modulus, psi	4350000
Poisson's ratio, [-]	0.26
Fluid viscosity, cp	5
Fracture height, ft	200
Injection time, min	60
Leak-off coefficient, ft/min ^{0.5}	0.001
Well spacing	600
Gauge length, m	10

In Figure 19, the cone shapes for four cases are displayed. The slope of the cone shape can be expressed as,

$$k = \frac{\Delta d}{\Delta t} \quad (19)$$

where d is the depth of the linear boundary front, and t is the time. Table 3 lists the slopes for all four cases.

Table 3—Slopes of cone shape pattern with different injection rates

Case	Injection rate, bbl/min	Slope, /
a	10	0.4211
b	15	0.3073
c	20	0.2182
d	25	0.1546

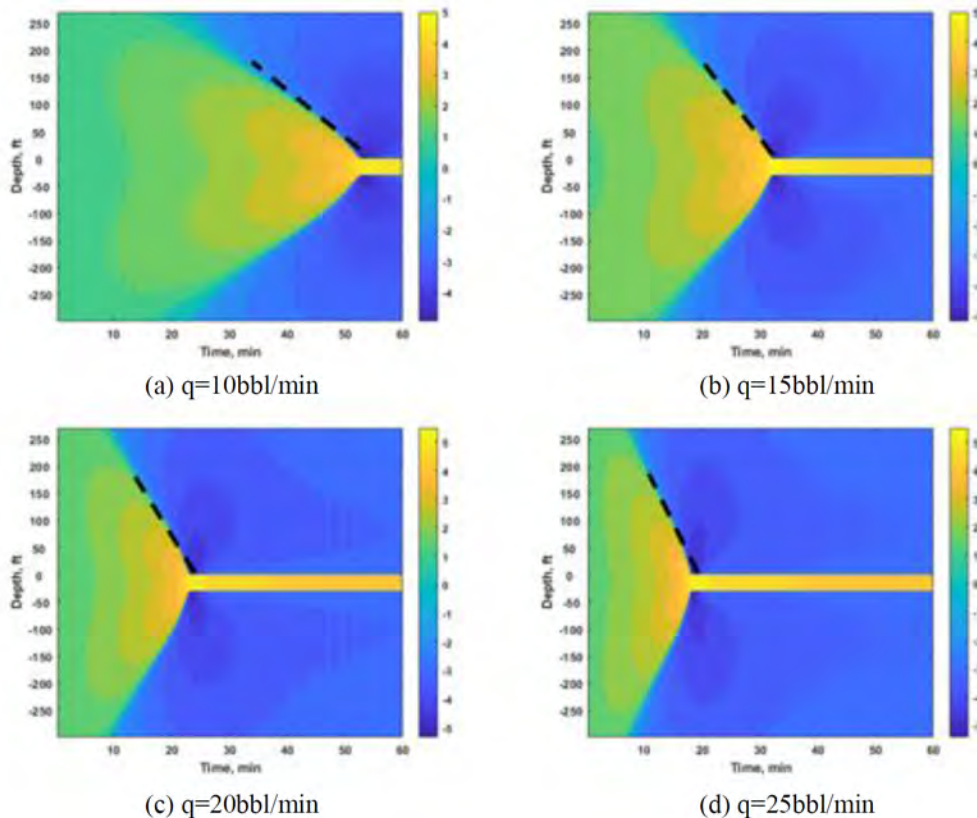


Figure 19—Different pattern slopes based on different injection rates

Plotting the slopes as a function of injection rate, Figure 20 shows that a simple linear relationship can be found between the fracture propagation front and the injection rate. From the numerical exercises, we observed that the linear correlation holds well when the injection rate is between 10 bbl/min to 25 bbl/min. This simple observation can help to identify the injection rate distribution in multiple fracture cases, and therefore understand fracture network development better.

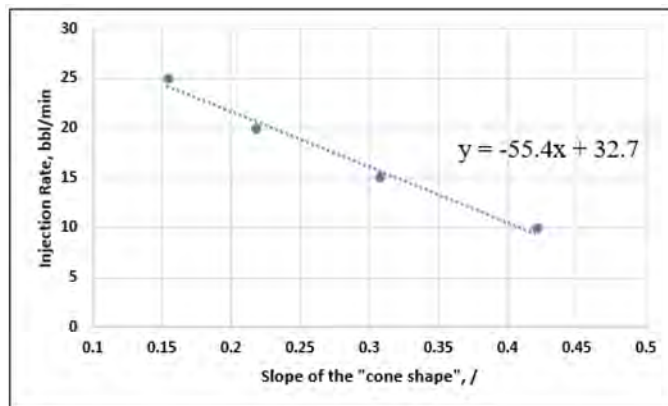


Figure 20—Linear correlation of different pattern slopes and different injection rates

Examples of Idealized Fracture Systems

Multiple fracture scenarios are examined in this study to identify the characteristics of strain rate responses as a function of injection rate distribution. We use a synthetic case that has 5 fractures, equally distanced along a horizontal well. Figure 21 shows the placement of the fractures. The fracture geometry is simulated

individually, but the stress, displacement, strain and strain rate are calculated in the system with the superposition principle. With all other parameters kept constant, injection rate distribution into each fracture is the only parameter examined in this study with the total injection rate fixed. Figure 21 shows the fracture system used for simulation, and Table 4 listed the input used for calculation.

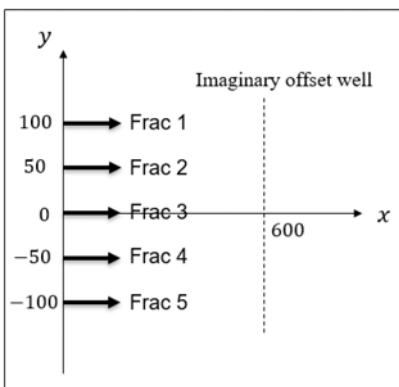


Figure 21—Simulation domain for idealized fracture systems study

Table 4—Input data for idealized fracture systems study

Parameter	Value
Young's modulus, psi	4350000
Poisson's ratio, [-]	0.22
Total injection rate per one side, bbl/min	45
Fluid viscosity, cp	5
Fracture height, ft	200
Injection time, min	60
Leak-off coefficient, ft/min ^{0.5}	0.001
Gauge length, m	2

Uniformed Injection Rate Distribution

The uniformed case is to evenly distribute the injection fluid to 5 fractures. As expected, for a homogeneous reservoir, the fractures propagate exactly the same way. With 5 equally sized fracture, the strain rate as a function of time is displayed in Figure 22. The strain rate response on the fiber optic sensor to fracture propagation shows an evenly distributed strain rate for all fracture.

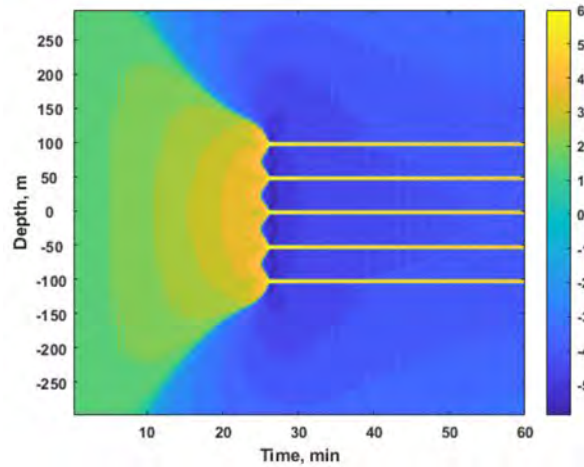


Figure 22—Characterization of strain rate responses for the uniformed distribution case

Side-Biased Injection Rate Distribution

In this synthetic case, we assume the fractures on one side of the center fracture take more fluid compared with the fractures on the other side. This simulates toe-bias or heel-bias case (since there is no flow in the wellbore, there is no difference for toe or heel in the example). Figure 23 shows the fluid distribution (left) and the strain rate response to the fracture propagation (right). Because of the biased distribution of injection fluid, the fractures propagate with different velocity; with the fractures take more fluid develop faster. If the fractures taking similar fluid locate next to each other, the cone shapes of the fractures are more likely connected (two fractures at the lower side and two fractures at the higher side). There is no significant slope difference for all cone shapes because the injection rate difference is small (15% versus 20% versus 25%).

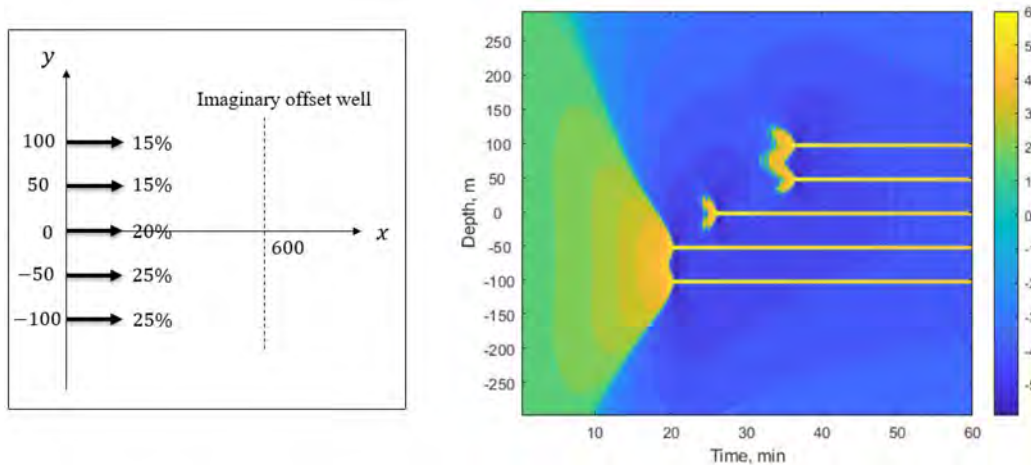


Figure 23—Characterization of strain rate responses for the side-biased distribution case

Center-Dominant Injection Rate Distribution

The center-dominant case assigns 30% of injection fluid to the center fracture, and 15% of fluid to each fracture at the end. The left picture of Figure 24 shows the injection fluid distribution, and the right picture shows the strain rate response for this distribution. Higher injection rate results in faster fracture propagation, smaller slope and large impacted area (center fracture). Because the fractures have similar rate are not located next to each other, the cone shapes do not connect to each other. The cone-shape pattern for 15% of the injection rate is very close to 20% of the injection rate.

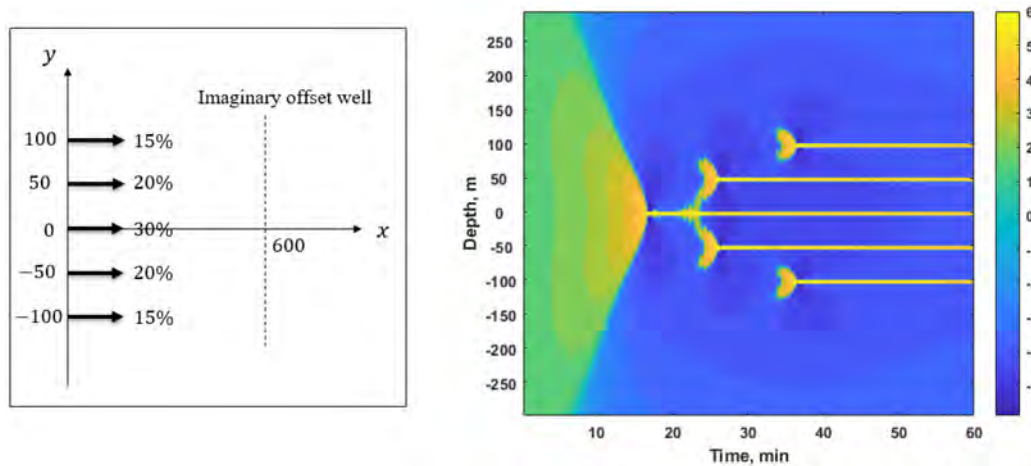


Figure 24—Characterization of strain rate responses for the center-dominant distribution case

U-Shaped Injection Rate Distribution

The U-shaped case assigns the most fluid to the end-fractures in a symmetric manner. Figure 25 shows the injection rate distribution and the strain rate response to the fracture propagation. The two end-fracture take 60% of the total injection. Even the distance between the fractures is large (200 ft), the cone shapes for the two fractures are connected. Center fracture generates the smallest cone in this case.

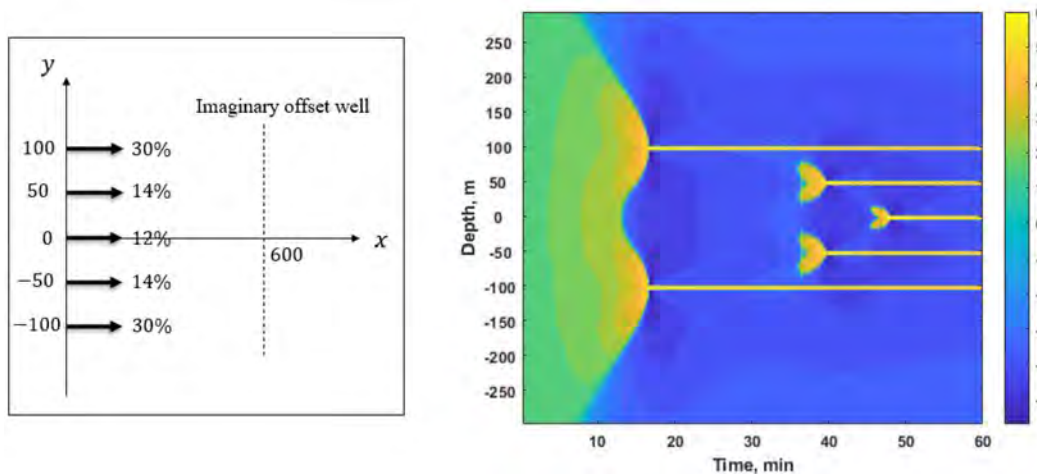


Figure 25—Characterization of strain rate responses for the U-shaped distribution case

Field Example

Even though the above examples are based on idealized patterns, the learnings from the analysis can be applied to the field case for prelim diagnosis. The strain responses for field cases are extremely complex with numerous impact parameters. Thus, no one monitoring data can interpret fracture network correctly. Combination of multiple monitoring methods can generate more comprehensive understanding of fracture network. In this study, we use high-frequency DAS and distributed temperature during warm-back at the injection well to generate the injection fluid distribution at the treated well (Pakhotina et al., 2020a). We attempt to confirm the fluid distribution generated by DAS and DTS at the injection well with the strain rate monitored by DAS at the monitoring well. The high-frequency DAS interpretation suggests a flow distribution for one stage pumping as shown in Figure 26. The other input data is listed in Table 5.

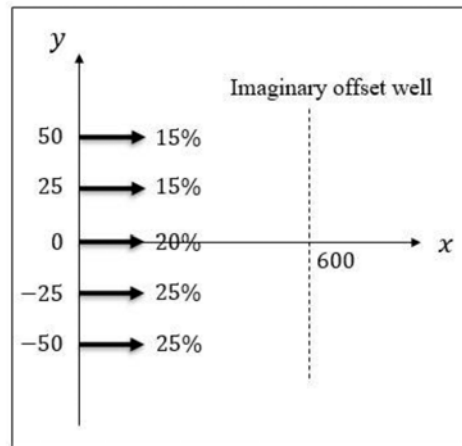


Figure 26—Assumed fluid distribution for strain rate simulation

Table 5—Input data for the field example study

Parameter	Value
Young's modulus, psi	2900000
Poisson's ratio, [-]	0.15
Total injection rate per one side, bbl/min	45
Fluid viscosity, cp	10
Fracture height, ft	100
Injection time, min	60
Leak-off coefficient, ft/min ^{0.5}	0.001
Well spacing, ft	600
Gauge length, m	8

Figure 27 shows the monitored data of strain rate by the fiber optic sensor (left) and model simulated strain rate (right). The highest injection fluid is assigned to two lower clusters because of the connection of the cone shape and the strip. The upper clusters take less fluid compared with the lower clusters, and arrive at the monitoring well at a later time. It is obvious that the solution of this approach is non-unique. It also does not have the resolution required to interpret fracture geometry. This is more true when the gauge length of the sensor is large. The result from the strain rate analysis by DAS can provide support to other monitoring interpretations.

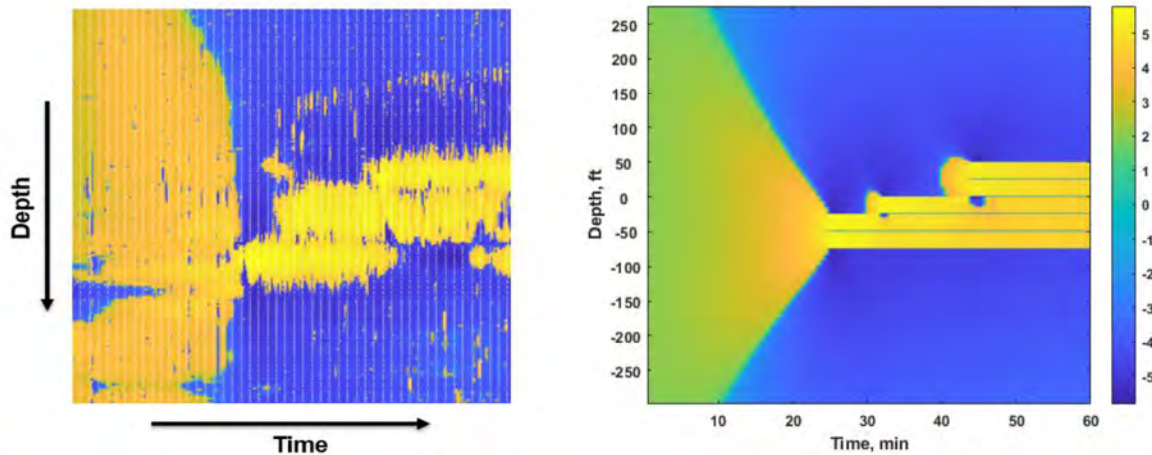


Figure 27—Comparison of fiber-measured strain rate (left) with simulated strain rate (right)

Conclusions

An integrated methodology has been developed to simulate both strain rate based on rock deformation theory and strain rate based on fiber-optic measurement during hydraulic fracturing. The approach is built for the scenario of a monitoring well with DAS in a vicinity of a well that is being fractured. The methodology is applied to synthetic examples to examine the connection between strain rate responses and fracture propagation during injection. The followings are concluded from the study.

1. Strain rate response to a fracture propagating towards the monitoring well where DAS is installed has a cone-shape front before intercept the monitoring well, and a strip-shape after passing the monitoring well.
2. The cone-shape slope is correlated to injection rate. Within certain range (10 bbl/min to 25 bbl/min in this study) the slope is inversely proportional to the injection rate. Based on this observation, injection fluid distribution can be estimated.
3. Low-frequency DAS recorded strain rate does not have the resolution to estimate fracture geometry since it is calculated based on an average value of displacements over the gauge length, especially when the gauge length is large. It is a good indicator of fracture extension and fracture front based on the shape change. Combined with other fiber optic measurements, DAS measured strain rate provides constrains on injection fluid distribution, helps in fracture characterization, and is a supplement to other monitoring methods for fracture geometry.

Nomenclature

D	Displacement discontinuity, ft
d	Depth of the linear boundary front, ft
E	Young's modulus, psi
G	Shear modulus, psi
G^n	Olson's factor, dimensionless
GL	Fiber optic cable gauge length, m
h	Fracture height, ft
j	Position in fiber, ft
k	Slope of the "cone shape", dimensionless
q	Injection rate, bbl/min
t	time, min
u	Displacement, ft

- ε Strain, dimensionless
- $\dot{\varepsilon}$ Strain rate, min^{-1}
- $\ddot{\varepsilon}$ Enlarged strain rate, dimensionless
- $\hat{\varepsilon}$ Log-transformed strain rate, dimensionless
- ν Poisson's ratio, dimensionless
- σ Stress, psi

References

- Bukhamsin, A. and Horne, R. 2014. Using Distributed Acoustic Sensors to Optimize Production in Intelligent Wells. Presented at the SPE Annual Technical Conference and Exhibition, Amsterdam, 27–29 October. SPE-170679-MS. <https://doi.org/10.2118/170679-MS>.
- Crouch, S. L. 1976. Solution of Plane Elasticity Problems by the Displacement Discontinuity Method. *International Journal for Numerical Methods in Engineering* **10**(2): 301–343.
- Crouch, S. L. and Starfield, A. M. 1983. *Boundary Element Methods in Solid Mechanics*. London, UK: George Allen and Unwin. <https://doi.org/10.1002/nme.1620191014>.
- Dou, S., Lindsey, N., Wagner, A.M. et al. Distributed Acoustic Sensing for Seismic Monitoring of The Near Surface: A Traffic-Noise Interferometry Case Study. *Sci Rep* **7**, 11620 (2017). <https://doi.org/10.1038/s41598-017-11986-4>.
- Jin, G., and B. Roy, 2017, Hydraulic-fracture geometry characterization using low-frequency DAS signal: *The LeadingEdge*, **36**, 975–980, <https://doi.org/10.1190/tle36120975.1>.
- Li, X., Zhang, J., Grubert, M., Laing, C., Chavarria, A., Cole, S., & Oukaci, Y. (2020, January 28). Distributed Acoustic and Temperature Sensing Applications for Hydraulic Fracture Diagnostics. Society of Petroleum Engineers. doi: [10.2118/199759-MS](https://doi.org/10.2118/199759-MS).
- Olson, J. E. 2004. Predicting fracture swarms- the influence of subcritical crack growth and the crack-tip process zone on joint spacing in rock. *Geological society, London, Special Publications* **231**(1): 73–88.
- Pakhotina, I., Sakaida, S., Zhu, D., & Hill, A. D.: "Diagnosing Multistage Fracture Treatments with Distributed Fiber-Optic Sensors." Paper presented at the SPE Hydraulic Fracturing Technology Conference and Exhibition, The Woodlands, Texas, USA, February 2020a. doi: <https://doi.org/10.2118/199723-MS>.
- Pakhotina, J., Zhu, D., & Hill, A. D. (2020b, October 21). *Evaluating Perforation Erosion and its Effect on Limited Entry by Distributed Acoustic Sensor DAS Monitoring*. Society of Petroleum Engineers. doi: [10.2118/201538-MS](https://doi.org/10.2118/201538-MS).
- Tang, J. 2021. *Pattern Generation of Strain Rate Simulation for Cross-Well Hydraulic Fracture Monitoring in Unconventional Reservoirs*. Ph.D. Dissertation. Texas A&M University.
- Ugueto C., G. A., Huckabee, P. T., Molenaar, M. M., Wyker, B., & Somanchi, K. (2016, February 1). *Perforation Cluster Efficiency of Cemented Plug and Perf Limited Entry Completions; Insights from Fiber Optics Diagnostics*. Society of Petroleum Engineers. doi: [10.2118/179124-MS](https://doi.org/10.2118/179124-MS).
- Ugueto, G. A., Todea, F., Daredia, T., Wojtaszek, M., Huckabee, P. T., Reynolds, A., ... Chavarria, J. A. (2019, September 23). *Can You Feel the Strain? DAS Strain Fronts for Fracture Geometry in the BC Montney, Groundbirch*. Society of Petroleum Engineers. doi: [10.2118/195943-MS](https://doi.org/10.2118/195943-MS).
- Valko, P., Economides, M. J. 1995. *Hydraulic fracture mechanics*. John Wiley & Sons Ltd, Baffins Lane, Chichester, West Sussex PO19 IUD, England.
- Wu, K. 2014. *Numerical Modeling of Complex Hydraulic Fracture Development in Unconventional Reservoirs*. Ph.D. Dissertation. The University of Texas at Austin.